Low-Thrust Propulsion and Drift Orbit Optimization for Multi-Client Servicing Missions in Low Earth Orbit

The Journal of the Astronautical Sciences (2026) 73:36
https://doi.org/10.1007/s40295-026-00580-4

RESEARCH

Low-Thrust Propulsion and Drift Orbit Optimization for Multi-Client Servicing Missions in Low Earth Orbit

Riccardo Apa[1] · **Jennifer Hudson**[2] · **Marcello Romano**[3]

Received: 5 June 2025 / Accepted: 25 February 2026

Abstract

This paper presents a general approach to solve multi-client space logistics path optimization problems in the case of low-thrust propulsion. The methodology accounts for key time-dependent factors, including secular J_2 and drag perturbations, eclipse propulsion constraints, and servicer fuel mass depletion. A low-thrust transfer strategy, consisting of three phases (thrust-coast-thrust), is employed, utilizing a drift orbit to correct the difference in Right Ascension of the Ascending Node. The drift orbit parameters are optimized by using a nonlinear programming algorithm to minimize the fuel cost associated with the transfer while satisfying a maximum time of flight constraint. An optimization is conducted for all possible transfers between the satellites of a dataset on a two-dimensional discrete grid of initial servicer mass and departure time. This procedure creates two four-variable arrays representing the cost of each possible visitation in terms of fuel consumption and time of flight. The arrays are then interpolated to efficiently solve a general path optimization problem by using a genetic algorithm. Two test cases are analyzed for datasets consisting of 12 and 20 satellites in low Earth orbit, respectively. The first addresses an optimal open tour problem where the servicer must visit all satellites once while minimizing total fuel consumption. The second addresses an on-orbit refueling problem where the servicer must refuel as many satellites as possible. The mission scenario is generalized to consider a priority index associated with each client; servicing time and fuel mass constraints are also taken into account.

Keywords Space trajectories · Multi-target mission · Low-thrust propulsion · Space logistics · Astrodynamics

List of Symbols

a	Semi-major axis (m)
C	Distance metric
$\mathcal{D}$	Set of satellite orbit IDs

Extended author information available on the last page of the article

Published online: 24 March 2026

$\Delta\theta$	True anomaly difference (rad)
Δt_{RV}	Phasing maneuver time (s)
ΔV	Velocity increment (m/s)
ΔV_{RV}	Phasing maneuver cost (m/s)
ToF	Time of flight (s)
$f_{\Delta V}$	Velocity increment bilinear interpolation function.
f_{ToF}	Time of flight bilinear interpolation function
i	Inclination (rad)
d	Satellite orbit ID (-)
Ψ	Combinatorial subproblem cost function
T_{op}	Problem refueling operation time (s)
I_{sp}	Specific impulse (s)
m_i	Initial mass (kg)
M_0	Discretization total wet mass (kg)
M_{dry}	Discretization dry mass (kg)
M_{fuel}	Problem fuel mass (kg)
W_i	Problem priority index (-)
M_{op}	Problem refueling operation mass (kg)
$T_{M,0}$	Discretization start time (s)
ΔT_M	Discretization total mission duration (s)
$\overline{d}$	Problem initial satellite orbit ID (-)
m	Mass (kg)
N	Number of discretization points (-)
f	Acceleration magnitude (m/s^2)
N_{gen}	Number of generations (-)
N_M	Number of initial mass discretization points (-)
N_d	Subset dataset size (-)
N_{pop}	Population size (-)
N_{run}	Number of runs (-)
N_{sat}	Number of satellites (-)
N_{stall}	Number of stall generations (-)
N_T	Number of departure time discretization points (-)
Ω	Right ascension of the ascending node (rad)
p	Distance metric parameters
t_i	Departure time (s)
t	Time (s)
T	Control thrust vector (N)
$\mathcal{T}$	Set of control thrust functions
T_{max}	Maximum available thrust (N)
t_0	Mission start time (s)
C_D	Drag coefficient (-)
S	Reference aerodynamic surface(m^2).
ToF	Time of flight vector (s)
X	State of the satellite
V	Orbital velocity magnitude (m/s)
w_{ecl}	Eclipse factor (-)

Z_{eq} Equality constraints
Z_{ineq} Inequality constraints

Subscripts

D Drift orbit value
err Error value
min Minimum value
max Maximum value
opt Optimal value
val Validation value
tot Total sequence value

1 Introduction

Over the past decades, various mission types involving servicer spacecraft visiting multiple orbital locations have been proposed and analyzed. Space logistics is defined as the theory and practice of driving space system design for operability and supportability, and of managing the flow of materiel, services, and information needed throughout a space system lifecycle[1].

In-space Servicing, Assembly, and Manufacturing (ISAM) [1] and on-orbit fuel depot positioning missions [2] are among the application areas of greatest interest to space logistics. These missions involve multiple rendezvous maneuvers between the servicing satellite and multiple client satellites to address operational needs, including satellite inspection (e.g., health and status monitoring), repairs (e.g., mechanical assistance for proper deployment), and refueling. Another research area of great interest concerns orbital debris mitigation. Different solutions have been proposed to reduce the amount of debris in Low Earth Orbit (LEO); many of them involve the use of an active spacecraft performing a close approach to a set of debris. Finally, some data-collecting missions can be mathematically modeled as a multiple visitation problem, where a probe satellite must visit specific points in space to conduct observations. Given the limited resources available on-board the servicer satellite, path optimization tools are crucial for efficiently addressing these problems while satisfying operational constraints. Path optimization problems involving multiple rendezvous with moving targets are referred to as *Moving-Target (or time-dependent) Traveling Salesman Problems* (MTTSPs). These problems typically fall into the class of Nondeterministic Polynomial-time hard (NP-hard) problems [3]; their combinatorial complexities mainly lie in the mixed integer/continuous nature of the variables involved and the proper definition of a distance metric quantifying the cost (propellant, time, or a combination of the two [4, 5]) associated with each individual visiting maneuver (leg). By adopting the term *client* to refer to the orbital states that the servicer must visit, a path optimization problem can be formulated as a nonlinear time-dependent problem composed of two subproblems [6]:

[1] AIAA Space Logistics Technical Committee website, https://www.aiaa-sltc.org/.

I. A functional subproblem, where the cost of each maneuver (*distance metric* or *leg cost function*) is computed by solving an optimal control problem.
II. A combinatorial subproblem involving the generation of the sequence of clients to visit.

Even considered separately, these two subproblems are difficult to solve. Concerning the functional subproblem, analytical solutions exist only in very simple cases and are mainly distinguished on the basis of the type of propulsion, the orbital perturbations included in the model, the inclusion of the servicer fuel mass depletion, and the objective function [7, 8]. The functional optimization problem is usually easier to solve when the servicer is endowed with high-thrust propulsion because of the smaller number of variables [4, 9–11]. However, the use of high-thrust propulsion for multiple rendezvous requires a huge amount of fuel, limiting its application to a small number of clients. To mitigate this issue, Cerf [11] considers a passive correction of the Right Ascension of the Ascending Node (RAAN) by exploiting a drift orbit to reduce fuel consumption. An optimal sequence for visiting four client satellites with minimal fuel consumption is found. The adoption of low-thrust propulsion has been proposed as a viable alternative strategy for servicing a larger number of clients [12–20]. Given the problem's complexity, the studies referenced above make specific assumptions about the functional and/or combinatorial subproblems to obtain a solution. A multiple-visitation optimal tour problem for a very large dataset of asteroids is solved by Gatto and Casalino [12]. However, the distance metric adopted assumes small differences between the orbital elements of the satellites. Furthermore, the servicer fuel mass depletion is neglected. Li et al. [13] adopts a similar distance metric, which includes the secular J_2 perturbation in the model. The fuel mass depletion effect is addressed through empirical formulas. The optimal tour solution for an active debris removal mission is obtained. Both studies, however, disregard the effects of drag and propulsion limitations during eclipse phases. Narayanaswamy et al. [14] solves the combinatorial subproblem by using a distance metric which neglects time-dependent factors. The optimal sequence trajectories are then determined through a six-element-targeting feedback controller. A three-phase distance metric including the effects of drag, eclipse propulsion constraint, servicer fuel mass depletion and propulsion system duty cycle to obtain the cost and the associated trajectories of a debris removal mission is considered by Wijayatunga et al. [15]. Jorgensen and Sharf [16] addresse a similar problem, where the functional subproblem is solved using an algorithm based on Nonlinear Programming (NLP). The six-element targeting trajectory is determined for a five-piece active debris removal mission. However, these studies do not address the combinatorial subproblem (i.e., the sequence is not optimized). A solution of an optimal tour problem for an active debris removal mission is presented by Zuiani and Vasile [18]. The distance metric is derived by assuming an in-plane control acceleration in order to reduce the number of optimization parameters. Averaged dynamics equations and fixed-parameter

drift orbits are adopted to solve the functional subproblem. However, propulsion constraints due to eclipse phases are not considered. Cerf [21] addresses an active debris removal mission involving the removal of 15 objects across three separate missions, considering both high-thrust and low-thrust propulsion. The single-target problem is solved through a three-phase maneuver strategy, wherein a two-parameter drift orbit is optimized–under fixed departure and arrival times–to minimize RAAN correction costs. All possible visitation costs are precomputed and stored to construct a response surface model, which is subsequently embedded within the combinatorial subproblem. This latter is solved using a simulated annealing algorithm. However, the model neglects eclipses, atmospheric drag, and the servicer mass variation–factors that can significantly affect the accuracy of the single-target solution, particularly for electric low-thrust propulsion. Lee and Ahn [19] propose a two-phase framework for solving the multi-target rendezvous problem, combining high-thrust and low-thrust trajectories via an extended Q-law from Varga and P´erez [22]. Applied to an open tour involving eight satellites in nearly circular LEO, the method first computes single-target maneuver costs across various departure times, then solves the combinatorial problem using Integer Linear Programming (ILP). However, the framework does not account for servicer mass and drag effects in maneuver cost calculations, and its reliance on ILP restricts its applicability to problems with linear objective functions and constraints. Apa et al. [23] presents a general approach to solving multi-client space logistics problems by employing a feedback controller to address the functional subproblem. To reduce the combinatorial complexity, a data interpolation method is used, and the proposed methodology is tested on a dataset of 20 satellites in Medium Earth Orbit (MEO) and Geostationary Earth Orbit (GEO). However, the simulations are limited to solving an optimal open tour problem and do not address more complex scenarios, such as on-orbit refueling problems, where operational constraints–such as the mass and time required for servicing operations–play a critical role. While the approach considers primary orbital perturbations, it does not leverage the secular J_2 perturbation to optimize fuel-efficient trajectories, a factor that is particularly relevant for LEO missions. By expanding from previous research [21, 23], this study introduces a general methodology applicable to a broad class of mission scenarios involving multi-target visitation problems under low-thrust propulsion in LEO. In order to solve the functional subproblem, we adopt a three-phase maneuver distance metric similar to that employed by Wijayatunga et al. [15] which takes into consideration the effects of servicer fuel mass depletion, drag, Earth-shadow eclipse, and secular J_2. A fast NLP derivation of the single-target problem is used to find a two-parameter drift orbit that satisfies the operational constraints while minimizing the cost associated with active RAAN correction. All possible visitation costs are then computed for a discrete number of servicer mass and departure time. Bi-linear interpolation is applied to obtain a quick-to-evaluate continuous approximation of the distance metric. A genetic algorithm is finally run multiple times to ensure conver-

gence to the global optimal sequence. Two application cases exemplify the proposed methodology.

The main contribution of this work lies in the introduction of a general framework for efficiently solving a broad class of time-dependent multi-client path optimization problems under diverse nonlinear operational constraints, with application to low-thrust scenarios in LEO. The proposed framework accounts for key time-dependent factors–secular J_2 perturbations, eclipse power constraints, atmospheric drag, and the servicer's fuel mass depletion–while including two-parameter drift orbit optimization to maximize mission profitability. This is achieved without resorting to problem linearization. The paper is organized as follows. In Sect. 2 the problem is stated; Sect. 3 presents the distance metric adopted; Sect. 4 presents the time-varying matrix interpolation approach; in Sect. 5 the combinatorial subproblem and the algorithm used to determine the optimal sequence are presented; Sect. 6 exemplifies the approach on two test cases; finally, in Sect. 7 the conclusions are drawn.

2 Path Optimization Problem Formulation

The MTTSP represents the archetype of multiple-visitation problems, where a salesman must visit all cities of a dataset once and only once. The cost of each visitation is quantified by a time-dependent function, and the optimal sequence is the one minimizing the sum of the costs. Path optimization problems constitute a broader category of problems that incorporate general constraints and objective function formulations [6]. The global optimization problem can be mathematically formulated by combining integer variables, continuous variables, and functions. Let N_{sat} be the number of satellites considered. Let $\mathcal{D} = \{d_1, \ldots, d_i, \ldots, d_{N_d}\}$, where $d_i \in \{1, \ldots, N_{sat}\}$, be a set of positive integers whose elements are the IDs of the $N_d \leq N_{sat}$ satellites to be visited. Let $\mathrm{ToF} = [t_1, \ldots, t_i, \ldots, t_{N_d}]$, where $t_i \in \mathbb{R}^+$, be a vector of real numbers containing the time of each rendezvous, and let $\mathcal{T} = \{\mathrm{T}_1(t), \ldots, \mathrm{T}_i(t), \ldots, \mathrm{T}_{N_d-1}(t)\}$ be a set of functions where $\mathrm{T}_i(t)$ represents the control law to perform the i^{th} visitation (e.g., $\mathrm{T}_i(t)$ is the quantity associated with the solution of the functional subproblem). Finally, let t_0 be the start time of the mission. Denoting with $\mathcal{K} = \{1, \ldots, N_d\}$ and $\mathcal{M} = \{1, \ldots, N_d - 1\}$, the path optimization problem can be stated as follows [23]

Problem 1 Path Optimization Problem

$$\min_{\mathcal{D},\mathrm{ToF},\mathcal{T}} \sum_{i=1}^{N_d-1} C_i \left(d_i, d_{i+1}, t_i, t_{i+1}, \mathrm{T}_i(t), \mathrm{p}\right)$$

subject to

$$
\begin{aligned}
&\dot{\mathrm{X}}_S(t) = \mathcal{F}\left(\mathrm{X}_S(t), \mathrm{T}_i(t)\right) \forall t \in \left[t_0, t_{N_d}\right], \forall i \in \mathcal{M} \\
&\|\mathrm{T}_i(t)\| \leq T_{max} \forall t \in \left[t_0, t_{N_d}\right], \forall i \in \mathcal{M} \\
&\dot{\mathrm{X}}_i(t) = \mathcal{G}_i\left(\mathrm{X}_i(t), \mathrm{T}_i^c(t)\right) \forall t \in \left[t_0, t_{N_d}\right], \forall i \in \mathcal{K} \\
&\mathrm{X}_S(t_0) = \mathrm{X}_{S,0} \\
&\mathrm{X}_i(t_0) = \mathrm{X}_{i,0} \forall i \in \mathcal{K} \\
&\mathrm{X}_{S,[1:6]}(t_i) = \mathrm{X}_{d_i,[1:6]}(t_i) \forall i \in \mathcal{K} \\
&t_i \leq t_{i+1} \forall i \in \mathcal{M} \\
&\mathrm{Z}_{eq}(\mathcal{D}, \mathrm{X}_S, \mathrm{X}_1, \ldots, \mathrm{X}_{N_d}, \mathrm{ToF}, \mathcal{T}) = 0 \\
&\mathrm{Z}_{ineq}(\mathcal{D}, \mathrm{X}_S, \mathrm{X}_1, \ldots, \mathrm{X}_{N_d}, \mathrm{ToF}, \mathcal{T}) \leq 0
\end{aligned}
$$

where T_{max} is the maximum available thrust of the servicer. $C_i\left(d_i, d_{i+1}, t_i, t_{i+1}, T_i(t), \mathrm{p}\right)$ denotes the cost of going from satellite d_i at time t_i to satellite d_{i+1} at time t_{i+1} using the control law $\mathrm{T}_i(t)$, and p is a vector of parameters (e.g., propulsion system specific impulse, servicer coefficient of drag, etc.). $\mathrm{X}_S(t) = [a(t), e(t), i(t), \Omega(t), \omega(t), \theta(t), m(t)]_S^\intercal$ is the state of the servicer, where $a(t)$ is the semi-major axis, $e(t)$ the eccentricity, $i(t)$ the inclination, $\omega(t)$ the argument of perigee, $\Omega(t)$ the RAAN, $\theta(t)$ the true anomaly, and $m(t)$ is the mass; while $\mathrm{X}_i(t)$ represents the state of the i^{th} client. $\mathcal{F}$ and $\mathcal{G}_i$ represent the dynamics of the servicer and the dynamics of i^{th} client, respectively. They are functions of the state and the control thrust acting on the satellite ($\mathrm{T}_i(t)$ or $\mathrm{T}_i^c(t)$). $\mathrm{X}_{S,0}$ and $\mathrm{X}_{i,0}$ denote the initial boundary conditions, while $\mathrm{X}_{S,[1:6]}(t_i) = \mathrm{X}_{d_i,[1:6]}(t_i)$ represents the rendezvous condition between the servicer and the client d_i, with the subscript $[1:6]$ indicating that only the first six components must be the same at time t_i. Finally, Z_{eq} and Z_{ineq} represent other nonlinear equality or inequality constraints involving the optimization variables, and the state of the satellites. Problem 1 was intentionally formulated in a general form to represent a broad class of problems and to capture the common features typically associated with time-dependent multi-client optimization scenarios. Depending on the specific mission case and its underlying assumptions, both the set of variables involved and their relationships may vary. Consequently, the specific form of the dynamics $\mathcal{F}$ and $\mathcal{G}_i$, as well as other factors expressed through Z_{eq} and Z_{ineq} (e.g., fuel mass exchange, maximum mission duration), can only be properly defined once the particular scenario is specified.

Figure 1 shows a schematic representation of a multi-client mission involving five satellites. Due to operational constraints, such as fuel capacity limitations, it is generally not feasible to reach all clients in the dataset. In this example, the servicer departs from orbit 1 and visits the client satellites identified by IDs 3 and 5, resulting in the visiting sequence $\mathcal{D} = \{1, 3, 5\}$. The total mission cost is expressed as $C_1 + C_2$. For clarity, Fig. 1 does not depict multiple revolutions, which are characteristic of low-thrust propulsion, nor drift orbits, both of which are considered in this work (see Sect. 3).

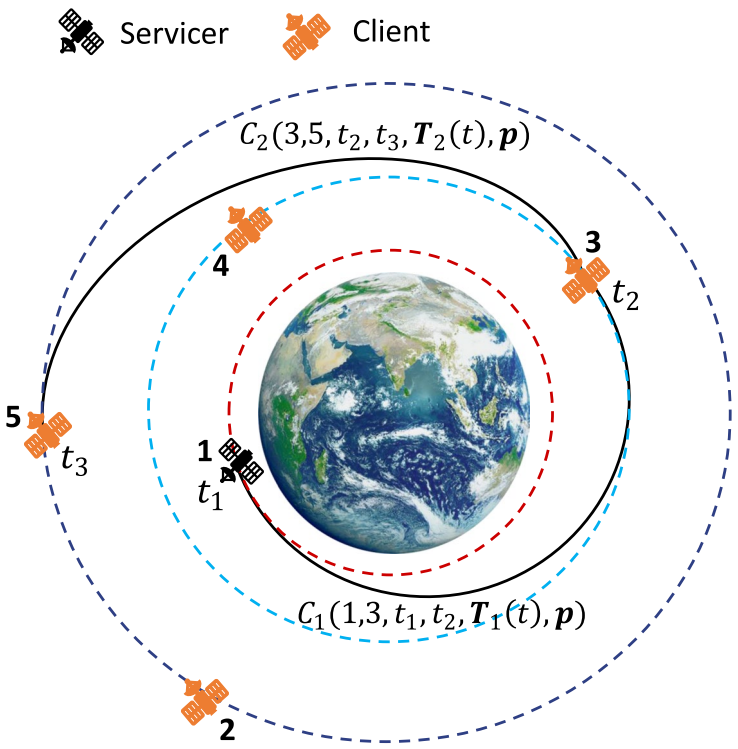

Fig. 1 Schematic representation of servicer trajectory for a multi-client mission

Problem 1 is defined by the choice of a distance metric and an algorithm to solve a problem involving a mix of integer variables, real variables, and functions. In the following, the dependence of the distance metric on the parameters p will be assumed and will not be explicitly indicated.

3 Functional Subproblem

A distance metric $C\left(d_i, d_j, t_i, t_j, \mathrm{T}_{i\to j}(t)\right)$, which quantifies the cost of transferring from satellite orbit d_i to d_j, with departure at time t_i and arrival at time t_j ($t_j \geq t_i$), must be defined. The functional subproblem then reduces to finding the control law $\mathrm{T}_{i\to j}(t)$ by using results from optimal control theory [24]. Some approximations are necessary to reduce the computational burden. The following assumptions are here adopted:

Assumption 1 Servicer trajectory and client orbits are nearly circular ($e \leq 0.05$).

Assumption 2 Phasing maneuver cost is neglected. It has been demonstrated that the cost difference between a transfer maneuver and a rendezvous maneuver is generally negligible in the case of low-thrust propulsion [25]. This is a standard assump-

tion when dealing with multiple-visitation low-thrust problems [14, 17, 26, 27]. The impact of this assumption is evaluated in Sect. 6.5.

Assumption 3 The transfer cost between any ordered pair of satellites is determined solely by their initial orbital states. Under this assumption, a distance metric C can be defined beforehand for each possible transfer [6, 14, 19, 21].

By considering the servicer equipped with a low-thrust propulsion system and the assumptions above, a three-phase maneuver is adopted [11], consisting of:

1. Transfer from initial state to a drift orbit.
2. Drift orbit.
3. Transfer from the final state of the drift orbit to the final orbit.

The cost of the transfer is represented by the total velocity increment $\Delta V = \Delta V_1 + \Delta V_2 + \Delta V_3$ (where the subscripts indicate the phase they refer to) applied by the servicer's propulsion system to transfer the spacecraft from the initial orbit to the target orbit.

Figure 2 shows a schematic example of a three-phase maneuver in the case of near-circular orbits. In the first phase, the servicer is transferred from its initial orbit (a_i,i_i,Ω_i) to a drift orbit defined by its semi-major axis a_D and inclination i_D. During the second phase, the RAAN difference is corrected by using differential precession,

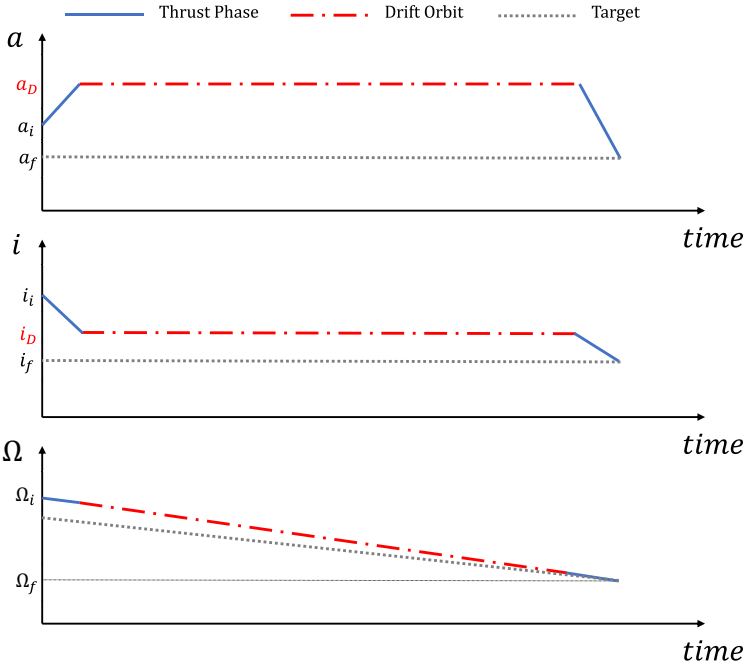

Fig. 2 Three-phase maneuver schematic example

while propulsion is employed solely to counteract the drag effect. In the final phase, the satellite is transferred to the target orbit (a_f,i_f,Ω_f). Drag, propulsion constraints due to eclipse phases, and fuel mass depletion effects will be considered during the three phases. By selecting the optimal drift orbit parameters (a_D, i_D), and using constant-thrust transfers to and from the drift orbit, an optimal thrust control strategy is defined. The duration of the constant-thrust arcs in phases 1 and 3 define the optimal thrust control timing.

3.1 Three-Phase Maneuver Transfer

The computations for the ΔV in Phases 1 and 3 are based on the results presented in [15, 28–30] and derived using the averaged dynamics equations (see Appendix). During these phases, the servicer is transferred from the initial state (a_i, i_i, Ω_i) to the final state (a_f, i_f, Ω_f), where the semi-major axis and inclinations (a and i) are actively corrected through an in-plane maneuver while the RAAN varies according to the following equation [31]

$$\dot{\Omega}(t) = -\frac{3}{2} J_2 \sqrt{\frac{\mu}{a(t)^3}} \left(\frac{R_e}{a(t)} \right)^2 \cos i(t) \tag{1}$$

where $\mu = 3.986 \times 10^{14}$ m^3/s^2 is the gravitational constant, $J_2 = 1.083 \times 10^{-3}$ is the first zonal harmonic coefficient, and $R_e = 6378.137$ km is the Earth's equatorial radius. Given $a(t)$, $i(t)$, and Ω_i, Ω_f is obtained by integrating Eq. (1) from t_i to t_f

$$\Omega_f = \Omega_i - \int_{t_i}^{t_f} \frac{3}{2} J_2 \sqrt{\frac{\mu}{a(t)^3}} \left(\frac{R_e}{a(t)} \right)^2 \cos i(t) dt \tag{2}$$

In [30], the results presented in [28, 29] are extended to incorporate the effects of secular J_2, eclipse, and fuel mass depletion through a numerical procedure. With minor adaptations, the same algorithm can also consider the effects of drag [15]. The algorithm for computing the ΔV in Phases 1 and 3 is outlined in Algorithm 1. Notably, the algorithmic steps in Algorithm 1 follow the formulation originally derived in [30], which was later adapted as the *Extended Edelbaum method* in [15] to include aerodynamic drag. Algorithm 1 incorporates a slight revision compared to the version presented in [15]. In particular, the computation of the drag effect (steps 17 and 18) has been updated, and the corresponding influence on the instantaneous acceleration (step 19) has been included. Specifically, in steps 17 and 18, the drag effect is now evaluated at the midpoint between two time steps, t_k and t_{k+1}, rather than solely at t_k. It is worth noting that the drag calculation explicitly accounts for the variation of atmospheric density with altitude using an exponential model [32].

Given: t_i, a_i, a_f, i_i, i_f, Ω_i, m_i, I_{sp}, $T_{\max}$, ρ_0, H_0, C_D, S, N

$V_i = \sqrt{\frac{\mu}{a_i}}$, $V_f = \sqrt{\frac{\mu}{a_f}}$, $\Delta i = i_f - i_i$, $f_t = \frac{T_{\max}}{m_i}$

$\Delta V_f = \sqrt{V_i^2 + V_f^2 - 2V_iV_f\cos\left(\frac{\pi}{2}\Delta i\right)}$

$\beta_0 = \arctan\left(\frac{\sin\left(\frac{\pi}{2}\Delta i\right)}{\frac{V_i}{V_f} - \cos\left(\frac{\pi}{2}\Delta i\right)}\right)$

$t_f = \frac{\Delta V_f}{f_t} + t_i$, $\Delta t = \frac{t_f - t_i}{N-1}$

for $k = 1$ to N **do**

  $t_k = t_i + (k-1)\Delta t$

  $\Delta V_k = (t_k - t_i) f_t$

  $a_k = \frac{\mu}{V_i^2 + f_t^2 t_k^2 - 2V_i f_t t_k \cos(\beta_0)}$

  $V_k = \sqrt{\frac{\mu}{a_k}}$

  $i_k = i_i + \frac{2\,\mathrm{sgn}(\Delta i)}{\pi} \times$
  $\times \left(\arctan\left(\frac{\Delta V_k - V_i\cos\beta_0}{V_i \sin\beta_0}\right) + \frac{\pi}{2} - \beta_0\right)$

  $\beta_k = \arctan\left(\frac{V_i \sin(\beta_0)}{V_i\cos(\beta_0) - \Delta V_k}\right)$

end for

$\Omega_1 = \Omega_i$, $m_1 = m_i$

for $j = 1$ to $N-1$ **do**

  $w_{ecl} = w_{ecl}(t_j, a_j, i_j, \Omega_j)$ from [33]

  $m_{j+1} = m_j e^{-\frac{\Delta V_j}{I_{sp} g_0}}$

  $\overline{m} = \frac{m_j + m_{j+1}}{2}$

  $\overline{f}_d = \frac{S\rho_0 C_D}{2} \times \frac{1}{2} \times$
  $\times \left(\frac{V_j^2}{m_j} e^{-\frac{a_j - R_e}{H_0}} + \frac{V_{j+1}^2}{m_{j+1}} e^{-\frac{a_{j+1} - R_e}{H_0}}\right)$

  $f_{t,j} = \frac{T_{\max}}{\overline{m}} - \overline{f}_d \cos\left(\frac{\beta_j + \beta_{j+1}}{2}\right)$

  $t_{j+1} = t_j + \frac{\Delta V_{j+1} - \Delta V_j}{f_{t,j} w_{ecl}}$

  $\dot{\Omega}_j = -\frac{3}{2} J_2 \sqrt{\frac{\mu}{a_j^3}} \left(\frac{R_e}{a_j}\right)^2 \cos i_j$

  $\Omega_{j+1} = \Omega_j + \dot{\Omega}_j (t_{j+1} - t_j)$

end for

Return: ΔV_f, $\Delta t = t_N - t_i$, $\Delta\Omega = \Omega_N - \Omega_i$

Algorithm 1 Minimum-time two-orbital-element targeting $(a_i, i_i) \rightarrow (a_f, i_f)$

Algorithm 1 requires the spacecraft's initial mass m_i, the specific impulse I_{sp} of the propulsion system, the maximum thrust $T_{\max}$, the atmospheric density ρ_0 at reference height H_0, the coefficient of drag of the servicer C_D, its reference aerodynamic surface S, and the number of discretization points N. $T_{\max}$ is assumed to be constant, so the maximum available thrust acceleration increases as fuel is depleted and the servicer's mass decreases. The function $\mathrm{sgn}(\cdot)$ indicates the signum function, while $w_{ecl}(t, a, i, \Omega)$ is the function computing the eclipse mean time per orbit. In this study, the effect of Earth-shadow eclipses is taken into account, and w_{ecl} is evaluated following the methodology outlined in [33]. The gravity at Earth's surface is $g_0 = 9.80665$ m/s^2. The outputs are the total ΔV_f, the updated time of flight Δt, and the total RAAN variation $\Delta\Omega$ in the presence of perturbations. Note that the transfer strategy reported in Algorithm 1 allows a two-orbital-element targeting maneuver ($(a_i, i_i) \rightarrow (a_f, i_f)$). RAAN correction is performed during the intermediate phase, where differential precession due to secular J_2 is exploited (Eq. (1)). In this work, a circular two-parameter drift orbit is considered, defined by its semi-major axis a_D (or the associated velocity V_D) and inclination (i_D). The total servicer RAAN variation is the sum of the three phases (i.e., $\Delta\Omega_{tot} = \Delta\Omega_1 + \Delta\Omega_2 + \Delta\Omega_3$). The phasing time Δt_2 is computed to match the final client RAAN. The sum of these three sequences allows for a three-orbital-element targeting transfer $(a_i, i_i, \Omega_i) \rightarrow (a_f, i_f, \Omega_f)$, where the total time of flight $ToF = \Delta t_1 + \Delta t_2 + \Delta t_3$ depends on the parameters reported in Algorithm 1 and on the drift orbit parameters. Algorithm 2 delineates the three-phase maneuver computational steps to reach the final orbit. The algorithmic formulation is based on the results originally presented in [6, 11], which were later extended as the *RAAN matching method* in [15] to include aerodynamic drag effects

through steps 5–7. Step 4, which differs from previous versions, introduces the modulus function, $\mathrm{mod}(\cdot, 2\pi)$, to properly handle the periodic nature of the RAAN difference, while $\Omega_{c,i}$ represents the RAAN of the client at the initial time t_i.

Given: t_i, a_i, a_f, i_i, i_f, Ω_i, m_i, I_{sp}, $T_{\max}$, ρ_0, H_0, C_D, S, N, $\Omega_{c,i}$, a_D, i_D

1: Compute ΔV_1, Δt_1 and $\Delta\Omega_1$ from Algorithm 1 to transfer the servicer from initial orbit to the drift orbit $(a_i, i_i) \rightarrow (a_D, i_D)$

2: Compute ΔV_3, Δt_3 and $\Delta\Omega_3$ from Algorithm 1 to transfer the servicer from the drift orbit to the final orbit $(a_D, i_D) \rightarrow (a_f, i_f)$

3: Compute the total RAAN variation of the servicer and the client during phases 1 and 3

$$\Delta\Omega_S = \Omega_i + \Delta\Omega_1 + \Delta\Omega_3$$
$$\Delta\Omega_c = \Omega_{c,i} + \dot{\Omega}_c(\Delta t_1 + \Delta t_3)$$

4: Compute Δt_2 needed to match the RAAN difference

$$\Delta t_2 = \frac{\mathrm{mod}(\Delta\Omega_c - \Delta\Omega_S, 2\pi)}{\dot{\Omega}_D - \dot{\Omega}_c}$$

if $\Delta t_2 < 0$

$$\Delta t_2 = -\frac{\mathrm{mod}(2\pi - \Delta\Omega_c - \Delta\Omega_S, 2\pi)}{\dot{\Omega}_D - \dot{\Omega}_c}$$

where $\dot{\Omega}_D$ and $\dot{\Omega}_c$ are computed from Eq. (1)

$$\dot{\Omega}_D = -\tfrac{3}{2} J_2 \sqrt{\tfrac{\mu}{a_D^3}} \left(\tfrac{R_e}{a_D}\right)^2 \cos i_D$$

$$\dot{\Omega}_c = -\tfrac{3}{2} J_2 \sqrt{\tfrac{\mu}{a_f^3}} \left(\tfrac{R_e}{a_f}\right)^2 \cos i_f$$

5: Compute servicer mass at the beginning of phase 2

$$m_D = m_i e^{-\frac{\Delta V_1}{I_{sp} g_0}}$$

6: Compute drag acceleration during the phase 2

$$f_{d,2} = \frac{S\rho_0 C_D}{2} \frac{\mu}{a_D m_D} e^{-\frac{a_D - R_e}{H_0}}$$

7: Compute ΔV_2 to counteract the drag

$$\Delta V_2 = \int_0^{\Delta t_2} f_{d,2} dt$$

Return: $\Delta V = \Delta V_1 + \Delta V_2 + \Delta V_3$, $ToF = \Delta t_1 + \Delta t_2 + \Delta t_3$

Algorithm 2 Three-phase maneuver $(a_i, i_i, \Omega_i) \rightarrow (a_f, i_f, \Omega_f)$

It is important to note that the effect of J_2 on the client orbit is assumed to be constant, as all clients are located at fixed altitudes and inclinations. Conversely, the J_2 effect on the servicer is time-varying, due to changes in altitude and inclination during its continuous-thrust maneuvers in Phases I and III (see Algorithm 1). Figure 3 shows, in the Earth-Centered Inertial (ECI) reference frame, the orbital configuration associated with the three-phase maneuver. The servicer low-thrust trajectory is shown in grey, highlighting its characteristic multi-revolution behavior. Typically, the drift-orbit parameters in Phase 2 are selected so that most of the RAAN correction occurs during this phase (i.e., $\Delta\Omega_2 \gg \Delta\Omega_1$ and $\Delta\Omega_2 \gg \Delta\Omega_3$).

Finally, Algorithm 2 provides two quantities (ΔV and *ToF*). Once the characteristics of the propulsion system and the inertial properties of the servicer have been chosen, the ΔV and *ToF* required for a three-phase maneuver transfer can be expressed as follows

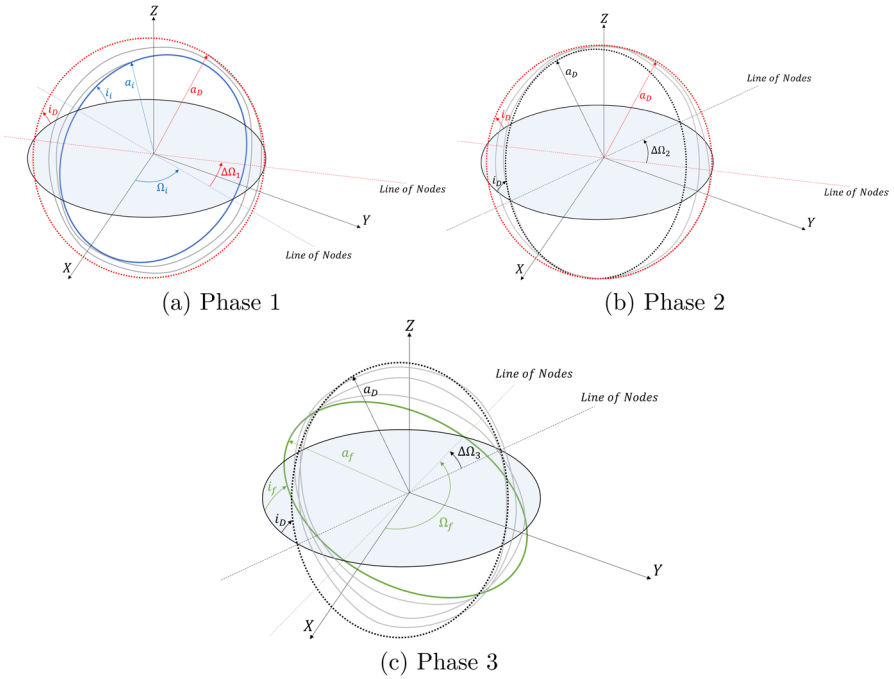

(a) Phase 1 (b) Phase 2

(c) Phase 3

Fig. 3 Three-phase maneuver orbital configuration in the ECI frame

$$\begin{aligned} \Delta V &= \Delta V\left(t_i, m_i, d_j, d_k, a_D, i_D\right) \\ ToF &= ToF\left(t_i, m_i, d_j, d_k, a_D, i_D\right) \end{aligned} \tag{3}$$

where t_i represents the initial time of the transfer, m_i the servicer initial mass, while a_D and i_D are the drift orbit parameters. The initial and target orbit states have been reduced to two integer variables, d_j and d_k, respectively. Given a dataset of N_{sat} satellites defined by their initial Keplerian elements at the start time t_0, it is possible to uniquely associate an integer l with each of them, ranging from 1 to N_{sat}. If the dynamics $\dot{\mathrm{X}}_l(t)\ \forall t$ are known, the complete state at time t_i can be obtained as

$$\mathrm{X}_l(t_i) = \mathrm{X}_l(t_0) + \int_{t_0}^{t_i} \dot{\mathrm{X}}_l(t)dt \tag{4}$$

where $\mathrm{X}_l(t_0)$ is the state of the l^{th} satellite at the start time. In conclusion, from t_i, d_j and d_k and Eq. (4), it is possible to obtain a_i, i_i, Ω_i, a_f, i_f and $\Omega_{c,i}$ needed by Algorithm 2 to compute the transfer cost to visit the satellite identified by d_k starting from the satellite identified by d_j departing at time t_i.

3.2 Drift Orbit Parameter Optimization

The drift orbit parameters a_D and i_D are two additional variables in the functional subproblem. In this work, these parameters have been optimized in order to minimize the ΔV of the transfer. A constraint on the maximum time of flight ToF_{max}

must be included to ensure a well-posed problem [11, 15]. Other constraints may include maximum and minimum values for the drift orbit parameters, denoted as $(a_{D,max}, i_{D,max})$ and $(a_{D,min}, i_{D,min})$, respectively. These constraints arise from various considerations such as drag effects. Based on Eq. (3), the problem of minimizing ΔV reduces to a constrained nonlinear optimization problem as outlined in Problem 2.

Problem 2 Drift Orbit Parameters Optimization

$$\begin{gathered}\min_{a_D, i_D} \Delta V\left(t_i, m_i, d_j, d_k, a_D, i_D\right) \\ \text{subject to} \\ a_{D,min} \leq a_D \leq a_{D,max} \\ i_{D,min} \leq i_D \leq i_{D,max} \\ ToF\left(t_i, m_i, d_j, d_k, a_D, i_D\right) \leq ToF_{max}\end{gathered}$$

The solution to the above problem provides the optimal drift orbit parameters ($a_{D,opt}$,$i_{D,opt}$), the minimum ΔV, and the associated time of flight

$$\Delta V_{opt} = \Delta V_{opt}\left(t_i, m_i, d_j, d_k\right) = \Delta V\left(t_i, m_i, d_j, d_k, a_{D,opt}, i_{D,opt}\right) \tag{5}$$

$$ToF_{opt} = ToF_{opt}\left(t_i, m_i, d_j, d_k\right) = ToF\left(t_i, m_i, d_j, d_k, a_{D,opt}, i_{D,opt}\right) \tag{6}$$

Equations (5) and (6) represent the solution of the functional subproblem considering the assumptions detailed in Sect. 3.1, including effects of servicer fuel mass depletion, eclipse constraints, drag, and a three-phase maneuver with optimal drift orbit parameters. A distance metric in the form described in Sect. 2 (i.e., $C\left(d_i, d_j, t_i, t_j, \mathrm{T}_{i\to j}(t)\right)$) can be constructed from Eqs. (5) and (6).

4 Time-Varying Matrix Interpolation Approach

The Time-Varying Matrix Interpolation method is introduced as an efficient approach to handle the time-dependent nature of Problem 1 while ensuring reasonable computational costs [23].

The method consists of two phases:

1. Cost-array computation.
2. Bilinear interpolation.

This procedure generates surrogate models that provide computationally efficient solutions to the functional subproblem. As a result, Problem 1 is reformulated as a purely combinatorial optimization problem, which can be addressed effectively using algorithms such as the one detailed in Sect. 5.3.

4.1 Cost-Array Computation

By defining the continuous intervals $M_C = [M_{dry}, M_0]$ and T_C=$[T_{M,0}, T_{M,0} + \Delta T_M]$, where M_0 denotes the total wet mass of the servicer at the beginning of the mission, M_{dry} represents its dry mass, $T_{M,0}$ is the mission start time, and ΔT_M is the total mission duration, discrete sets M_D and T_D can be constructed by discretizing M_C and T_C into $N_M + 1$ and $N_T + 1$ points, respectively. Letting $\mathcal{N}_M = \{1, .., N_M + 1\}$ and $\mathcal{N}_T = \{1, .., N_T + 1\}$ denote the indexing sets of the discretization, the following equations hold

$$\begin{array}{c} M_D = \{M_1, \ldots, M_i, \ldots, M_{N_M+1}\} \\ T_D = \{T_1, \ldots, T_l, \ldots, T_{N_T+1}\} \end{array} \tag{7}$$

where

$$\begin{array}{ll} M_i = M_{dry} + (i-1)\frac{M_0 - M_{dry}}{N_M}, & \forall i \in \mathcal{N}_M \\ T_l = T_{M,0} + (l-1)\frac{\Delta T_M}{N_T}, & \forall l \in \mathcal{N}_T \end{array}$$

By evaluating the cost functions in Eqs. (5) and (6) over the discrete sets defined in Eq. (7), two 4-dimensional arrays, $\Delta V_{opt,iljk}$ and $ToF_{opt,iljk}$, are computed as follows

$$\Delta V_{opt,iljk} = \Delta V_{opt}(M_i, T_l, d_j, d_k), \forall i \in \mathcal{N}_M, \forall l \in \mathcal{N}_T, \forall j, k \in \{1, \ldots, N_{sat}\} \tag{8}$$

$$ToF_{opt,iljk} = ToF_{opt}(M_i, T_l, d_j, d_k), \forall i \in \mathcal{N}_M, \forall l \in \mathcal{N}_T, \forall j, k \in \{1, \ldots, N_{sat}\} \tag{9}$$

Since the problem is time-dependent, swapping d_j and d_k in Eqs. (8) and (9) leads to different results (i.e., $\Delta V_{opt,iljk} \neq \Delta V_{opt,ilkj}$ and $ToF_{opt,iljk} \neq ToF_{opt,ilkj}$). When $j = k$, the initial and final states coincide, resulting in $\Delta V = ToF = 0$. Consequently, the total number of optimizations required is given by

$$z = (N_M + 1)(N_T + 1)(N_{sat} - 1) N_{sat} \tag{10}$$

Equation (10) expresses the number of times the functional subproblem is solved within the proposed framework, regardless of the distance metric used. Equations (8) and (9) define the fuel and time-of-flight costs, respectively, derived from solving the functional subproblem for all possible transfers between satellites in a given dataset, considering a finite set of servicer initial masses and departure times.

4.2 Bilinear Interpolation

In a real mission scenario, both the servicer's initial mass and the departure time assume values within specified continuous intervals. By using the pre-computed arrays, two mapping functions, $f_{\Delta V,jk} : \mathbb{R}^2 \to \mathbb{R}$ and $f_{ToF,jk} : \mathbb{R}^2 \to \mathbb{R}$, are introduced to operate on the sub-matrices $\Delta V_{opt,jk} := \Delta V_{opt,iljk}, \forall i, l$ and $ToF_{opt,jk} := ToF_{opt,iljk}, \forall i, l,$

as outlined in Eqs. (11) and (12). These functions provide an approximation of the costs over the continuous intervals M_C and T_C, as defined in Sect. 4.1.

$$\Delta V_{C,jk} = \Delta V_{C,jk}\left(t_i, m_i, d_j, d_k\right) = f_{\Delta V,jk}\left(t_i, m_i, V_{opt,jk}\right), \forall t_i \in T_C, \forall m_i \in M_C \quad (11)$$

$$ToF_{C,jk} = ToF_{C,jk}\left(t_i, m_i, d_j, d_k\right) = f_{ToF,jk}\left(t_i, m_i, ToF_{opt,jk}\right), \forall t_i \in T_C, \forall m_i \in M_C \quad (12)$$

These mapping functions are defined for all possible satellite transfer pairs (i.e., $\forall j, k \in \{1, \ldots, N_{sat}\}$). In this study, $f_{\Delta V,jk}$ and $f_{ToF,jk}$ are implemented as bilinear interpolating functions [34].

5 Combinatorial Subproblem

The results presented in Sect. 4 introduce two models (Eqs. (11) and (12)), which provide an approximate solution to the functional subproblem. These models account for both the system dynamics and the control law, reducing Problem 1 to a combinatorial path optimization problem. Recalling the definition of the visitation sequence $\mathcal{D}$ given in Problem 1 (i.e., $\mathcal{D} = \{d_1, \ldots, d_i, \ldots, d_{N_d}\}$, where $d_i \in \{1, \ldots, N_{sat}\}$ and $N_d \leq N_{sat}$), the combinatorial path optimization problem can be formally stated as follows.

Problem 3 Combinatorial Path Problem

$$\min_{\mathcal{D}} \quad \sum_{j=1}^{N_d-1} \Psi_j\left(d_j, d_{j+1}, \Delta V_{C,j(j+1)}, ToF_{C,j(j+1)}\right)$$

subject to

$$\begin{aligned}
&T_{M,0} \leq t_{i,j} \leq T_{M,0} + \Delta T_M \forall j \in \{1, \ldots, N_d\} \\
&M_{dry} \leq m_{i,j} \leq M_0 \forall j \in \{1, \ldots, N_d\} \\
&\mathrm{Z}_{eq}(\mathcal{D}, t_{i,1}, \ldots, t_{i,j}, \ldots, t_{i,N_d}, m_{i,1}, \ldots, m_{i,j}, \ldots, m_{i,N_d}) = 0 \\
&\mathrm{Z}_{ineq}(\mathcal{D}, t_{i,1}, \ldots, t_{i,j}, \ldots, t_{i,N_d}, m_{i,1}, \ldots, m_{i,j}, \ldots, m_{i,N_d}) \leq 0
\end{aligned}$$

Here, Ψ_j represents a general cost function that explicitly depends on the visitation sequence elements and on the transfer costs characterizing the maneuver from orbit d_j to d_{j+1}. The quantities $t_{i,j}$ and $m_{i,j}$ denote the servicer's departure time and mass from orbit d_j, respectively. The constraints imposed on $t_{i,j}$ and $m_{i,j}$ ensure that these variables remain within the ranges employed to construct the cost arrays described in Sect. 4.1. Although not explicitly stated, both $\Delta V_{C,j(j+1)}$ and $ToF_{C,j(j+1)}$ are treated as functions of $(t_{i,j}, m_{i,j}, d_j, d_{j+1})$. Note that in Problem 3, the only optimization variable is $\mathcal{D}$, representing the visitation order. This leads to a significantly reduced problem complexity compared to Problem 1, where, in addition to $\mathcal{D}$, continuous variables and functions were included as optimization variables. Problem 3 can be adapted to address a wide range of practical mission scenarios by appropriately defining the objective function and specifying the equality and inequality constraints,

denoted by Z_{eq} and Z_{ineq}, respectively. In this work, this framework is employed to formulate an open tour problem and an on-orbit refueling problem.

5.1 Open Tour Problem

Problem 3 is reformulated as an optimal open tour problem, where the servicer, initially located in a specific orbit $\overline{d} \in \{1, ..., N_{sat}\}$, must visit all N_{sat} satellites exactly once while minimizing the total fuel consumption. By defining the sets $\mathcal{K} = \{1, \ldots, N_{sat}\}$ and $\mathcal{M} = \{1, \ldots, N_{sat} - 1\}$, the combinatorial path problem is stated as follows.

Problem 4 Open Tour Problem

$$\min_{\mathcal{D}} \quad \sum_{j=1}^{N_{sat}-1} m_{i,j} \left(1 - e^{-\frac{\Delta V_{C,j(j+1)}(t_{i,j}, m_{i,j}, d_j, d_{j+1})}{I_{sp} g_0}}\right)$$

subject to

$$\begin{aligned}
& t_{i,1} = T_{M_0} \\
& t_{i,j} \leq T_{M_0} + \Delta T_M \forall j \in \mathcal{K} \\
& m_{i,1} = M_0 \\
& m_{i,j} \geq M_{dry} \forall j \in \mathcal{K} \\
& t_{i,j+1} = t_{i,j} + ToF_{C,j(j+1)}\left(t_{i,j}, m_{i,j}, d_j, d_{j+1}\right) \qquad \forall j \in \mathcal{M} \\
& m_{i,j+1} = m_{i,j} e^{-\frac{\Delta V_{C,j(j+1)}(t_{i,j}, m_{i,j}, d_j, d_{j+1})}{I_{sp} g_0}} \forall j \in \mathcal{M} \\
& d_1 = \overline{d} \\
& d_j \neq d_k \forall j, k \in \mathcal{K}, j \neq k \\
& |\mathcal{D}| = N_{sat}
\end{aligned}$$

Here, $|\mathcal{D}|$ denotes the cardinality of the visiting sequence. The first four constraints correspond to the time and mass bounds defined in Problem 3, whereas the remaining ones can be derived from the general nonlinear expressions Z_{eq} and Z_{ineq} introduced therein.

5.2 On-Orbit Refueling Problem

Problem 3 is here reformulated as a modified version of the combinatorial *Knapsack Problem* [35]. In this formulation, the servicer, starting from a specific initial orbit $\overline{d} \in \{1, ..., N_{sat}\}$ and carrying a limited amount of fuel M_{fuel} (with M_{fuel} chosen such that $M_0 - M_{fuel} \geq M_{dry}$), aims at refueling as many clients as possible. The problem is generalized to account for the relative importance of each client, which is quantified by a priority factor W_i, where $W_i \in \mathbb{N}, \forall i \in \{1, ..., N_{sat}\}$. Additionally, servicing operations require a time T_{op} during which the servicer provides a

fixed amount M_{op} of fuel to the client. By defining the sets $\mathcal{K} = \{1, \ldots, N_d\}$ and $\mathcal{M} = \{1, \ldots, N_d - 1\}$, the problem can be stated as follows.

Problem 5 On-orbit Refueling Problem

$$\min_{\mathcal{D}} \quad \left(-\sum_{j=1}^{N_d} W_{d_j} \right)$$

subject to

$$\begin{aligned}
&t_{i,1} = T_{M_0} \\
&t_{i,j} \leq T_{M_0} + \Delta T_M \forall j \in \mathcal{K} \\
&m_{i,1} = M_0 \\
&m_{i,j} \geq M_0 - M_{fuel} \forall j \in \mathcal{K} \\
&t_{i,j+1} = t_{i,j} + ToF_{C,j(j+1)}\left(t_{i,j}, m_{i,j}, d_j, d_{j+1}\right) + T_{op} \forall j \in \mathcal{M} \\
&m_{i,j+1} = m_{i,j} e^{-\frac{\Delta V_{C,j(j+1)}\left(t_{i,j}, m_{i,j}, d_j, d_{j+1}\right)}{I_{sp} g_0}} - M_{op} \forall j \in \mathcal{M} \\
&d_1 = \overline{d} \\
&d_j \neq d_k \forall j, k \in \mathcal{K}, j \neq k \\
&|\mathcal{D}| \leq N_{sat}
\end{aligned}$$

5.3 Integer Optimization Algorithm

In order to solve the combinatorial problem, both deterministic and heuristic algorithms can be utilized. In this work, a genetic algorithm [36] with mutation is used to generate sequences satisfying the constraints specified in Problems 4 and 5. The genetic algorithm is configured with user-defined parameters: the population size N_{pop}, the maximum number of generations N_{gen}, and the maximum number of stall generations N_{stall}. After each generation, the sequence associated with the minimum cost is selected and saved in case of an improvement in the objective function.

In any case, a new population is created starting from the previous one; the process is showed schematically in Fig. 4 for the case when a set of eight satellites are to be visited once and only once.

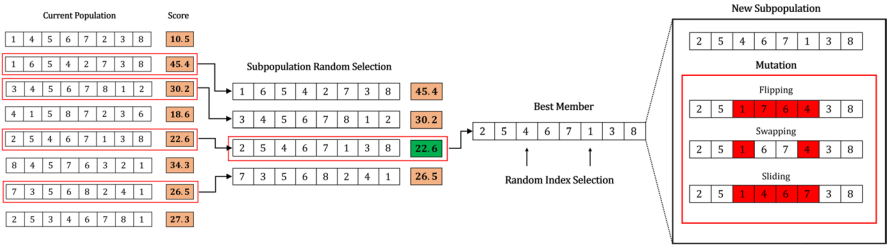

Fig. 4 New population creation example

Table 1 Satellites' initial Keplerian elements

ID	a(km)	i(deg)	Ω(deg)
Satellite - 1	7164.04	86.43	164.8
Satellite - 2	6989.20	86.44	151.3
Satellite - 3	7148.54	86.44	163.1
Satellite - 4	7159.28	86.41	157.9
Satellite - 5	7163.26	86.45	173.5
Satellite - 6	7123.77	86.42	154.0
Satellite - 7	7105.55	86.09	77.07
Satellite - 8	7142.54	86.39	147.4
Satellite - 9	7312.32	86.00	127.3
Satellite - 10	7048.23	86.23	62.44
Satellite - 11	7078.63	86.37	196.4
Satellite - 12	6945.29	86.14	7.535
Satellite - 13	7127.60	86.39	150.9
Satellite - 14	7064.04	87.55	56.76
Satellite - 15	6988.20	88.71	124.0
Satellite - 16	7144.54	87.09	74.86
Satellite - 17	7160.00	85.28	107.3
Satellite - 18	7163.30	85.81	117.1
Satellite - 19	7125.67	87.53	175.4
Satellite - 20	7305.55	89.52	174.0

Table 2 Aerodynamic and low-thrust propulsion servicer properties

Parameter	Unit	Value
Input power	kW	6.9
C_D	-	2
S	m^2	1.5
I_{sp}	s	4170
T_{max}	N	0.236

Given the current population, four members are randomly extracted, creating a subpopulation. The member associated with the best score is then selected to generate four new sequences. The first is the selected member itself, and the other three are created by flipping, swapping and sliding the elements contained in a subinterval. The subinterval is identified by two random integers extracted from a uniform distribution. The process is repeated until a new population of N_{pop} elements is created. The genetic algorithm terminates either when the maximum number of generations, N_{gen}, is reached, or when the objective function does not improve for N_{stall} generations.

6 Simulation Results

The proposed methodology was applied to two multiple-visitation case studies. Table 1 reports the initial orbital elements for all the satellites considered in this study, which are derived from the IRIDIUM constellation [14], and satisfy Assumption 1 (i.e., all orbits have $e \leq 0.05$). Specifically, Problem 4 was addressed using a data-

Table 3 NLP algorithm data

Parameter	Unit	Value
ρ_0	kg/m^3	2.34×10^{-13}
H_0	km	687.00
$a_{D,min}$	km	6728.14
$a_{D,max}$	km	7378.14
$i_{D,min}$	deg	0
$i_{D,max}$	deg	360
ToF_{max}	days	150
N	–	100

Table 4 Cost arrays computation data

Parameter	Unit	Value
Mission start date	–	01-*Jan*-2023
M_{dry}	kg	300
M_0	kg	700
$T_{M,0}$	days	0
ΔT_M	days	1650
N_M	–	11
N_T	–	22

set comprising the first 12 satellites from this table ($N_{sat} = 12$), while Problem 5 was solved using the full dataset of $N_{sat} = 20$ satellites. The specifications of the servicer's aerodynamic properties and low-thrust propulsion system, specifically the NEXT ion thruster [37], are reported in Table 2.

6.1 Solution of the Functional Subproblem

The three-phase maneuver with optimal drift orbit, as described in Sect. 3.1, was utilized to solve the functional subproblem. Cost arrays, computed using Eqs. (5) and (6), were generated for all possible transfers across two discrete intervals of initial servicer masses and departure times using the data provided in Tables 2, 3, and 4. With these tabulated values, the maximum velocity increment achievable by the servicer spacecraft is $\Delta V_{max} = I_{sp} g_0 \ln(M_0/M_{dry}) = 34.68$ km/s. The state of each satellite at time t_i was computed by propagating the initial Keplerian elements listed in Table 1 using Eq. (4). The propagation accounted for the secular J_2 perturbation (Eq. (1)) and assumed uncontrolled motion (i.e., $\mathrm{T}_i^c(t) = 0, \forall t$).

All the computations were conducted in MATLAB R2023a on a laptop equipped with an 11th Gen Intel(R) Core(TM) i7 2.3 GHz processor with 8 physical cores, running a 64-bit Windows operating system and 32 GB of RAM. The built-in function *fmincon* with the *interior-point* algorithm was employed to solve Problem 2, and the computation was parallelized using the MATLAB *parfor* keyword to specify parallel for-loops. In the twelve-satellite scenario, this procedure involved 36, 432 NLP optimizations (given by Eq. (10)) and took approximately 1.8 h. In the twenty-satellite scenario, 104, 880 NLP optimizations were performed, requiring a total computation time of 5.2 h.

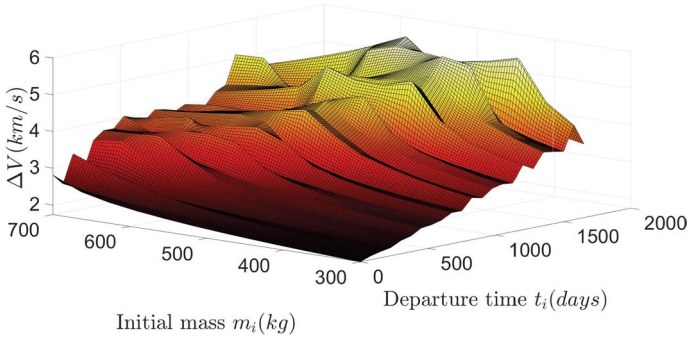

Fig. 5 $\Delta V_{C,jk}$ bilinear interpolation example, $j = 1$ and $k = 7$

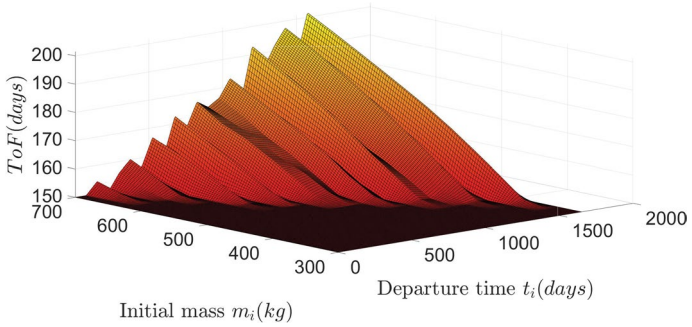

Fig. 6 $ToF_{C,jk}$ bilinear interpolation example, $j = 1$ and $k = 7$

6.1.1 Bilinear Interpolation Example

Figures 5 and 6 show an example of bilinear interpolation for the transfer between satellites 1 and 7 (see Table 1).

From Fig. 5, two main insights can be drawn. First, the required ΔV is consistently greater than 1 km/s, indicating a significant difference in Keplerian elements between the satellites. Second, the required ΔV generally increases with both increasing initial mass and departure time. This trend aligns with the fact that, for a fixed maximum thrust, lower masses lead to higher available acceleration, thus facilitating the transfer maneuver. Additionally, the increase in ΔV with departure time suggests that satellites are drifting apart due to differential node precession, making it more advantageous to visit the target satellite earlier in the mission when the difference in RAAN ($\Delta\Omega$) is smaller. Figure 6 highlights the feasibility of the transfer. For certain combinations of initial mass and departure time, the target can be reached within 150 days. However, when $\Delta\Omega$ is high and the available acceleration is low, no drift orbit exists that satisfies the constraints outlined in Problem 2. As we consider the effects of discretization on the interpolation process, it is clear that a finer discretization would increase both the accuracy of the bilinear interpolation and the computational

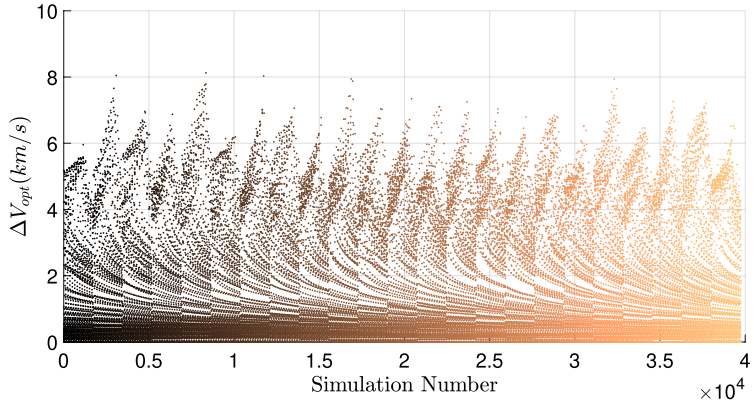

(a) ΔV_{opt} array inspection

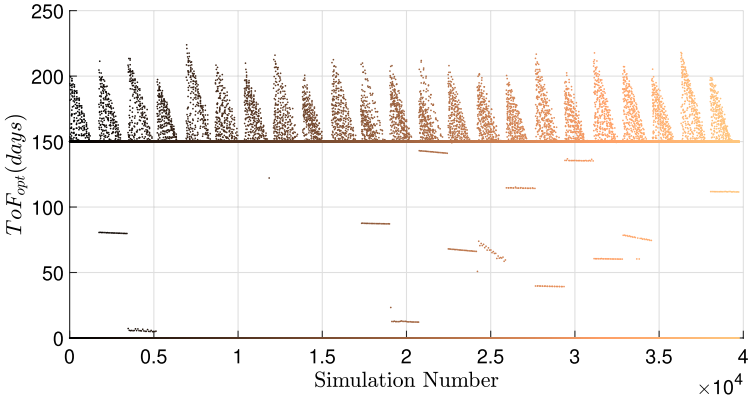

(b) ToF_{opt} array inspection

Fig. 7 Cost-array inspection

time required to create the $\Delta V_{opt,iljk}$ and $ToF_{opt,iljk}$, making the choice of N_M and N_T a trade-off between these two factors.

6.1.2 Cost-Array Inspection

Figure 7 shows the elements of $\Delta V_{opt,jk}$ and $ToF_{opt,jk}$ matrices for all $j, k \in \{1, \ldots, N_{sat}\}$ in the case of $N_{sat} = 12$. Each matrix element is identified on the abscissa axis. Simulations with the same initial mass and departure time are represented with the same color. The dependence on variables j and k (i.e., dependence on the initial and target orbits) can be observed from the variation along the vertical axis, where zero values associated with $j = k$ cases are also included. In Fig. 7a, most transfers show a cost ranging from 0.3 km/s to 4 km/s, while the most expensive transfers require an increment in velocity of about 8 km/s. This range of ΔV provides insights into the dispersion of Keplerian elements of satellites as the servicer's initial mass and departure time change. Nevertheless, the presence of high-cost transfers (up to 8 km/s) does not imply their selection in the final trajectory design. The solu-

tion of the combinatorial subproblem will discard such maneuvers in favor of visitation sequences composed of more efficient transfers.

From Fig. 7b, two main pieces of information can be captured. First, some transfers do not satisfy the maximum time of flight constraint. Second, most transfers converge to a solution requiring exactly the maximum time of flight ToF_{max}. This result is consistent with the considerations made in Sect. 3.2 concerning the well-posedness of the NLP problem.

6.2 Bilinear Interpolation Accuracy Analysis

The bilinear interpolation accuracy was evaluated using an alternative discretization of the M_C and T_C intervals for the twelve-satellite case. Two validation matrices ($\Delta V_{val,jk}$ and $ToF_{val,jk}$) were computed for all possible transfers, utilizing the same parameters as specified in Tables 2, 3, and 4, except for N_M and N_T, which were both set to $N_M = N_T = 6$. Defining the validation sets as $M_{D,val}$ and $T_{D,val}$, the percentage error for each sample (i.e., $\forall t_i \in T_{D,val}, \forall m_i \in M_{D,val}, \forall j,k \in \{1,\ldots,N_{sat}\}$) was calculated using the following equations

$$\Delta V_{err} = \frac{\Delta V_{C,jk} - \Delta V_{val,jk}}{\Delta V_{val,jk}} \times 100 \tag{13}$$

$$ToF_{err} = \frac{ToF_{C,jk} - ToF_{val,jk}}{ToF_{val,jk}} \times 100 \tag{14}$$

Figure 8 shows the results obtained for all samples, with the majority of percentage errors falling within the range of -5% to +5%. The distributions suggest that bilinear interpolation applied to the adopted discretization sets yields good estimations, as reflected by the statistical metrics: mean ($\mu_{\Delta V_{err}} = -0.198\%$) and standard deviation ($\sigma_{\Delta V_{err}} = 4.93\%$) for ΔV_{err}, and mean ($\mu_{ToF_{err}} = -0.102\%$) and standard

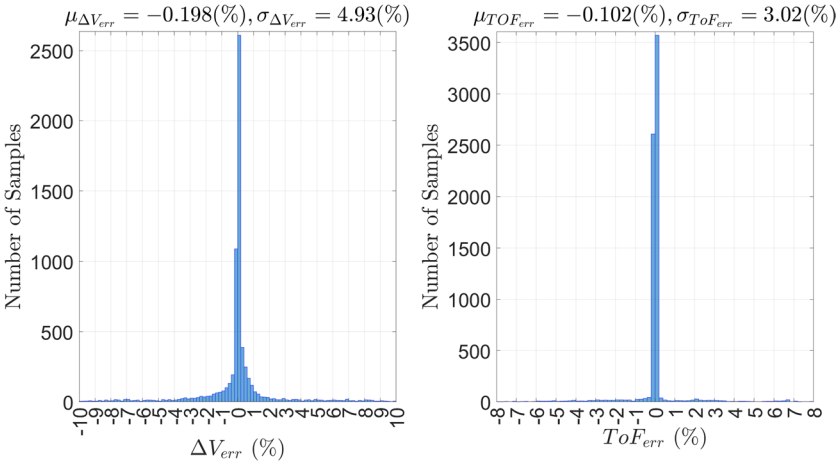

Fig. 8 Bilinear interpolation accuracy results

Table 5 Genetic algorithm simulation parameters

Parameter	Value
N_{pop}	100
N_{gen}	500
N_{stall}	50
N_{run}	100

Table 6 Optimal sequence results and validation: test case 1

Parameter	Unit	Value
$\mathcal{D}_{opt}$	–	{1, 2, 8, 6, 4, 3, 5, 11, 9, 7, 10, 12}
ΔM_{tot}	kg	115.43
ToF_{tot}	days	1437.6
$\Delta M_{tot,err}$	–	3.27%
$ToF_{tot,err}$	–	0.01%

deviation ($\sigma_{ToF_{err}} = 3.02\%$) for ToF_{err}. The accuracy can be further improved by using finer grids for initial masses and departure times.

6.3 Solution of the Combinatorial Subproblem

Problems 4 and 5 were solved using the genetic algorithm, as described in Sect. 5.3. The user-defined parameters for both application cases are reported in Table 5. The efficiency in evaluating the models $\Delta V_{C,jk}$ and $ToF_{C,jk}$ allows for running the algorithm multiple times to ensure convergence towards the global optimum, thus enhancing the reliability of the results. The genetic algorithm was executed N_{run} times per case in parallel, and the optimal sequence was selected as the best solution among all runs.

6.4 Test Case 1: Open Tour Problem

In this test case, the first twelve satellites from Table 1 are considered. The servicer is assumed to depart from satellite orbit 1 (i.e., $\overline{d} = 1$). The genetic algorithm took 44 s to find the optimal solution.

Table 6 reports the optimal sequence ($\mathcal{D}_{opt}$), the associated costs in terms of total fuel consumption (ΔM_{tot}) and total time of flight (ToF_{tot}), as well as the absolute percentage errors in total fuel consumption ($\Delta M_{tot,err}$) and total time of flight ($ToF_{tot,err}$). These errors were calculated by comparing the results with the values obtained by evaluating the optimal sequence using the non-approximated functions defined in Eqs. (5) and (6).

The servicer requires approximately four years to complete the mission, which is primarily due to the need to correct RAAN differences by employing drift orbits. In fact, the solution reveals that almost all visits employ the maximum allowable time of flight in the drift orbit (i.e., $ToF_{max} = 150$ days), which minimizes the ΔV consumption. Consequently, the mission requires a very low propellant mass, suggesting that shorter-duration missions could be feasible at the cost of higher fuel consumption. The low percentage errors observed validate the accuracy of the proposed methodology, aligning with the results presented in Sect. 6.2. The trajectories of the

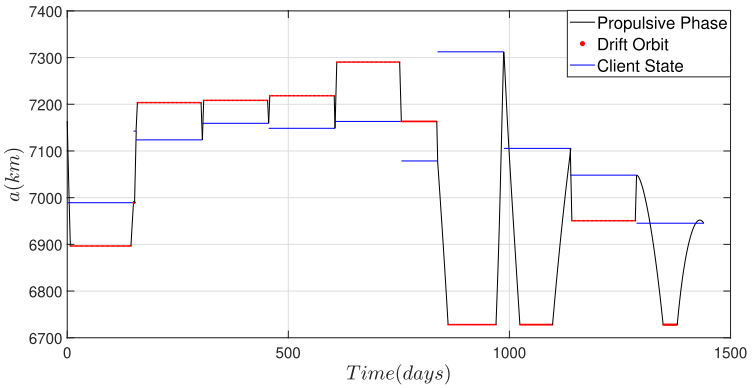

(a) Semi-major axis

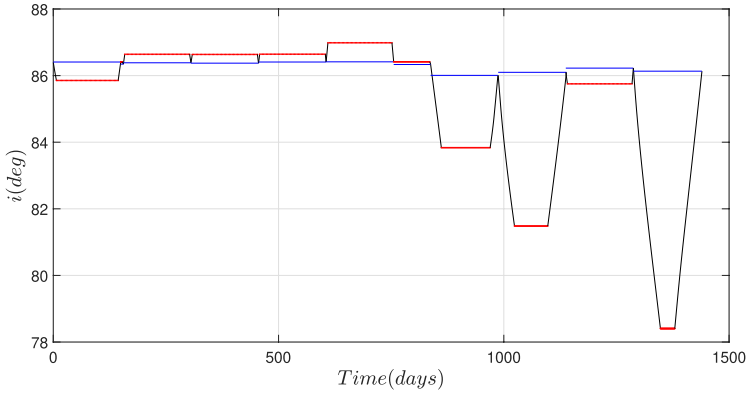

(b) Inclination

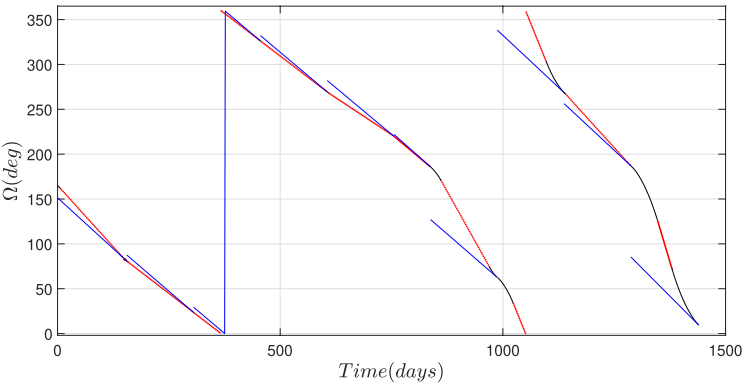

(c) Right Ascension of the Ascending Node

Fig. 9 Keplerian element trajectories: test case 1

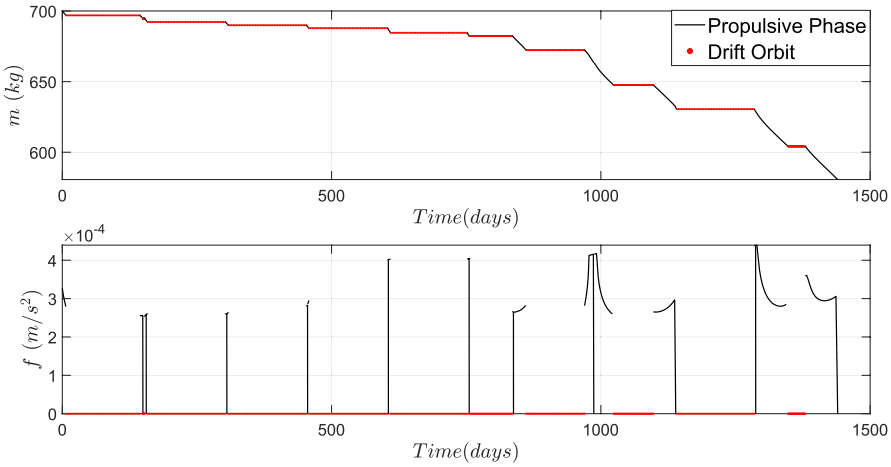

Fig. 10 Mass and acceleration magnitude histories: test case 1

Table 7 Simulation data for the on-orbit refueling problem

Parameter	Unit	Value
W_i	–	[0, 1, 3, 2, 3, 1, 3, 4, 2, 1, 2, 3, 2, 1, 3, 4, 1, 2, 3, 2]
M_{fuel}	kg	400
M_{op}	kg	25
T_{op}	days	10

optimal sequence, represented by the Keplerian elements (a, i, and Ω) for both the servicer and clients, are shown in Fig. 9. The three-phase maneuver structure is highlighted, and the RAAN precession of the client orbits is visible (see Fig. 9c). Notably, the clients are visited in a monotonically decreasing RAAN pattern. This behavior, referred to as *RAAN walk*, was initially identified in [38] for the time-independent case and is also observed in this time-dependent application.

The servicer mass and mean acceleration magnitude histories are shown in Fig. 10. During the phasing maneuvers, the mass is almost constant because control acceleration is applied only to counteract the drag. The mean acceleration is primarily influenced by the eclipse phases, which reduce the available acceleration and increase the transfer times of the propulsive phases.

6.4.1 Test Case 2: On-Orbit Refueling Problem

In this test case, the full satellite dataset reported in Table 1 is considered, with the servicer assumed to depart from satellite orbit 1 (i.e., $\overline{d} = 1$). Table 7 reports the simulation data for this application case, where the departure orbit is assigned a zero priority factor.

Table 8 Optimal sequence results and validation: test case 2

Parameter	Unit	Value
$\mathcal{D}_{opt}$	–	{1, 19, 5, 8, 4, 3, 9, 7, 16, 15}
ΔM_{tot}	kg	291.4
ToF_{tot}	days	1292.5
$\Delta M_{tot,err}$	–	0.03 %
$ToF_{tot,err}$	–	5.16×10^{-2} %

The genetic algorithm was employed with the parameters specified in Table 5 and adapted to consider the specific equality and inequality constraints of the problem. The algorithm converged in 36 seconds, revealing various optimal sequences with equivalent objective function values. The optimal sequence associated with the minimum fuel depletion is detailed in Table 8. The optimal sequence involves a refueling mission with 9 clients. The total fuel consumption is notably higher than that in the optimal tour test case. This outcome underscores how the choice of objective function can lead to significant differences in the optimal solution. As observed in the previous test case, the validation results show minimal percentage errors, highlighting the efficiency of the proposed method and the suitability of the discretization used in generating the cost arrays.

Figures 11, and 12 show the Keplerian elements trajectories (a, i and Ω) of both servicer and clients, and the servicer mass and mean acceleration histories, respectively. Servicing phases are also shown.

6.5 Effect of Perturbations and Phasing Maneuver Cost

This section analyzes the impact of perturbations on mission performance and provides an estimate of the phasing maneuver cost.

6.5.1 Effect of Eclipse and Drag

The influence of atmospheric drag and eclipse is assessed by re-evaluating the optimal sequences reported in Tables 6 and 8. The goal is to quantify the error introduced when these perturbations are neglected.

Specifically, the sequences in Tables 6 and 8 are re-analyzed using the distance metrics defined in Eqs. (5) and (6), which result from solving Problem 2 by setting $C_D = 0$ and $w_{ecl} = 1$ in Algorithm 1. Table 9 reports the results for both test cases and compares them to the nominal scenario where perturbations are included.

In test case 1, neglecting perturbations results in a fuel saving of approximately 16 kg, primarily due to the absence of correction maneuvers to counteract the drag. In test case 2, the difference is less than 2 kg, highlighting a lower sensitivity to perturbations. The difference between the two test cases arises from the number of targets visited–12 in test case 1 and 9 in test case 2–which directly affects the total total time of flight and thus the cumulative impact of drag. In both cases, the total time of flight remains nearly unchanged. This is expected, as also in this case the drift phase and transfer duration are optimized to maximize the use of ToF_{max}, thereby reducing RAAN correction costs via differential nodal precession.

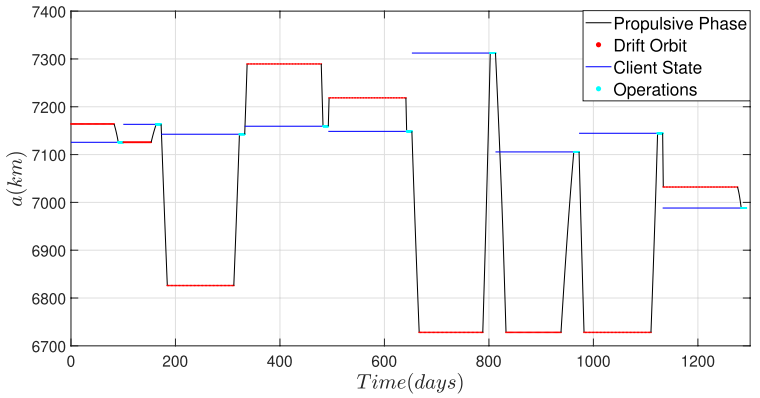

(a) Semi-major axis

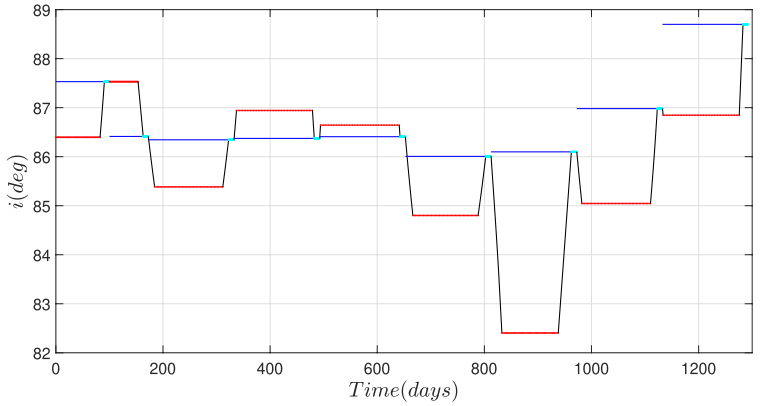

(b) Inclination

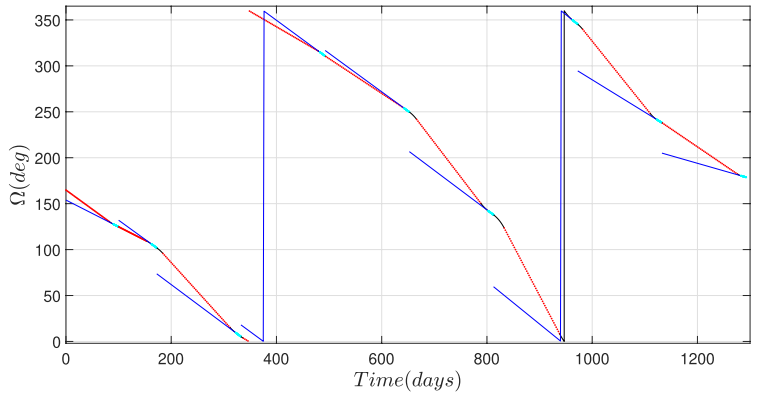

(c) Right Ascension of the Ascending Node

Fig. 11 Keplerian element trajectories: test case 2

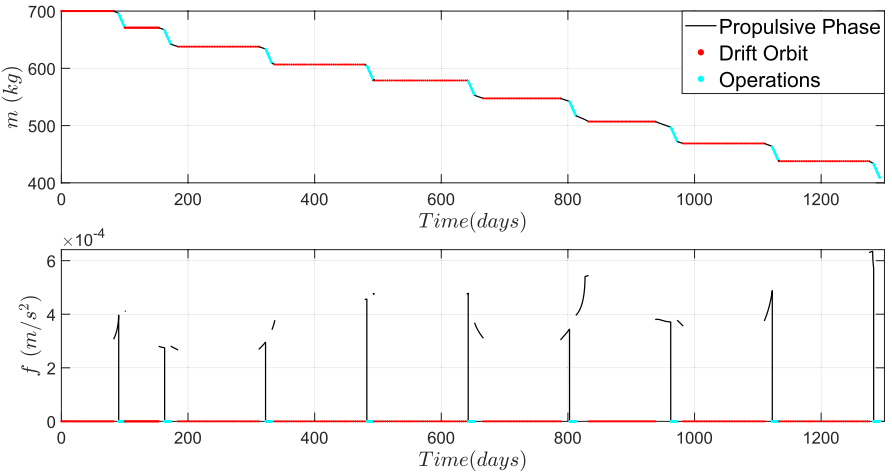

Fig. 12 Mass and acceleration magnitude histories: test case 2

Table 9 Effect of atmospheric drag and eclipse

Simulation	Test case 1		Test case 2	
	ΔM_{tot} (kg)	ToF_{tot} (days)	ΔM_{tot} (kg)	ToF_{tot} (days)
Perturbations included	119.3	1437.6	291.3	1292.5
Perturbations neglected	103.6	1441.7	289.4	1291.5

Figure 13 shows the servicer mass and control acceleration profiles for both test cases without perturbations. As in the nominal case, most of the time of flight is spent on drift arcs. The acceleration magnitude history increases linearly, as the continuous-thrust maneuvers are not affected by eclipse phases, and the mass decreases steadily due to propellant consumption. These results highlight the importance of accounting for perturbations, especially in highly dynamic environments such as LEO, to ensure accurate estimation of propellant consumption, which is critical for determining the optimal visiting sequence.

6.5.2 Estimation of Phasing Maneuver Cost

To assess the impact of neglecting the phasing maneuver costs (Assumption 2), an estimation is performed using the analytical approach proposed in [28], which provides the ΔV required for phasing between two satellites on the same orbit. Phasing is achieved by modifying the orbital period to compensate for a true anomaly difference, $\Delta\theta$, with the associated ΔV cost estimated as

$$\Delta V_{RV} = \frac{4\hat{a}}{3}\frac{\Delta\theta}{\Delta t_{RV}} \tag{15}$$

where $\hat{a}$ is the semi-major axis of the orbit, and Δt_{RV} is the time allocated for the phasing maneuver. The optimal sequences reported in Tables 6 and 8 were analyzed

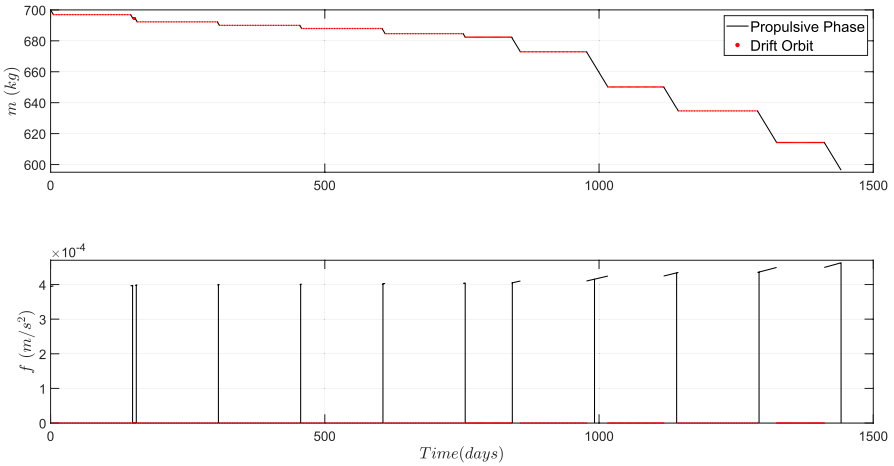

(a) Test case 1: open tour problem

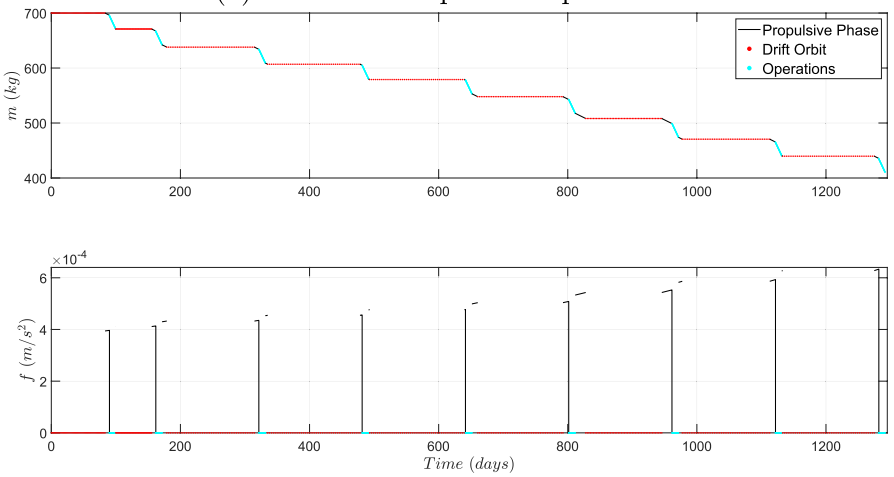

(b) Test case 2: on-orbit refueling problem

Fig. 13 Optimal sequence mass and acceleration magnitude histories, no perturbations

under two scenarios: $\Delta\theta = 90^\circ$ rad and $\Delta\theta = 180^\circ$ rad, the latter representing a worst-case condition. It is assumed that each phasing requires correcting the same angular separation after the orbital transfer (with $\hat{a}$ equal to the semi-major axis of the final orbit for each leg), and phasing times in the range $\Delta t_{RV} \in [5, 10]$ days are considered. Figure 14 shows the resulting percentage errors in total mass depletion and time of flight for both test cases. The results show that phasing duration significantly influences fuel consumption: shorter durations require larger semi-major axis changes to achieve the desired drift rate, leading to higher ΔV costs. In contrast, longer durations reduce fuel consumption but extend the total time of flight. However, for the scenarios considered, the errors in total fuel mass remain below 5% for test case 1 and 3% for test case 2. The higher error observed in test case 1 is attributable

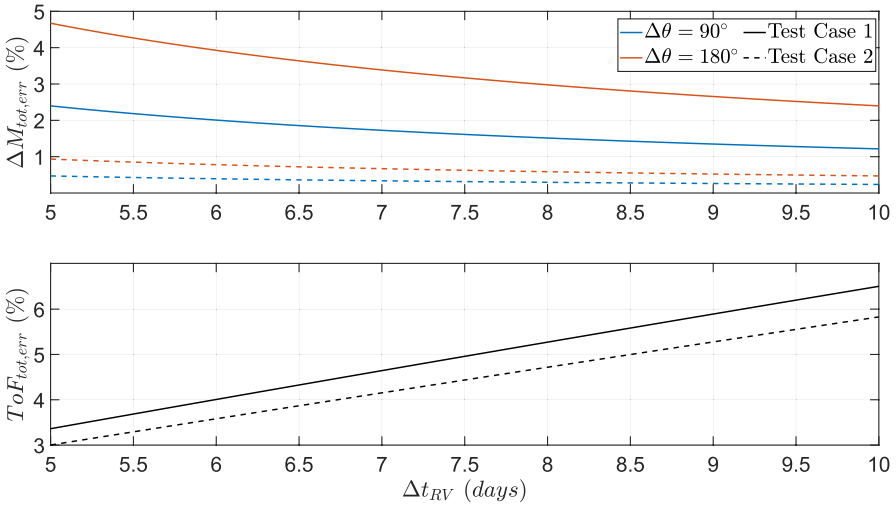

Fig. 14 Phasing maneuver cost error estimation

to the greater number of visited targets, which increases the cumulative cost of phasing maneuvers.

It is important to note that these results represent conservative estimates, as they assume the phasing maneuver occurs as a separate trajectory phase with maximum angular separation (i.e., $\Delta\theta = 180°$). In more realistic scenarios, where angular separations are typically smaller and phasing is integrated within the transfer arc, the associated cost is expected to be significantly lower.

7 Conclusion

In this work, we combine and expand approaches previously introduced [21, 23] to address space logistics problems involving low-thrust space trajectories. The general problem encompasses mixed integer/continuous and functional variables. The functional problem is first analyzed and solved by using a three-phase maneuver that considers the effects of secular nodal precession, drag, Earth-shadow eclipse, servicer fuel mass depletion, and a two-parameter optimal drift orbit. In order to address a generic path optimization problem, we used the Time-Varying Matrix Interpolation method. This approach involves two main steps: first, two arrays quantifying the ΔV and time of flight for each possible transfer are computed by solving the functional problem for discrete sets of initial servicer mass and departure times. Second, bilinear interpolation is applied to these arrays to derive continuous cost functions. The resulting combinatorial problem is then efficiently solved using a genetic algorithm. We demonstrate the effectiveness of this methodology through two application cases. The first involves an optimal open tour problem, where the servicer must visit all client satellites once, minimizing total fuel consumption. The second case focuses on on-orbit refueling, where the servicer aims at refueling as many satellites as possible, considering priority indices for each client, servicing time, and fuel

mass constraints. Results are presented for datasets consisting of twelve and twenty LEO satellites, respectively. The accuracy of the results is validated by comparing the optimal sequence total mass depletion and time of flight with those obtained by solving the non-approximated functional problem. The main computational challenge resides in computing the cost arrays. However, the algorithm is well-suited to parallel programming, enabling its application to large datasets. Moreover, once computed, these same cost arrays can be utilized to solve various path optimization problems considering multiple constraints across different mission scenarios when the same spacecraft is employed. Limitations arise solely from the assumptions made in addressing the functional problem.

Appendix A: Averaged Dynamics Equations

The averaged dynamics equations utilized in [28] are given by

$$\begin{aligned} \frac{\mathrm{d}i}{\mathrm{d}t} &= \frac{2f\sin\beta}{\pi V} \\ \frac{\mathrm{d}V}{\mathrm{d}t} &= -f\cos\beta \end{aligned} \tag{A1}$$

where f is the control acceleration, β is the thrust yaw angle (i.e., the angle between the thrust vector and the orbit plane), while i and V are the average inclination and orbital velocity magnitude of the satellite, respectively. The assumptions and the complete derivation of Eq. (A1) are detailed in [28].

Acknowledgements Mr Apa acknowledges the support of a doctoral fellowship funded by project NODES with funding from the MUR – M4C2 1.5 of PNRR funded by the European Union - NextGenerationEU (Grant agreement no. ECS00000036).

Author Contributions R.A. developed the methodology and performed the simulations. All authors analyzed the results and contributed to the interpretation of the data. R.A. wrote the main manuscript text. All authors reviewed and approved the final manuscript.

Funding Open access funding provided by Politecnico di Torino within the CRUI-CARE Agreement.

Data Availability No datasets were generated or analysed during the current study.

Declarations

Conflict of interest The author declares that there exists no competing financial interest or personal relationships that could have appeared to influence the work reported in this paper.

References

1. ISAM Interagency Working Group: National in-space servicing, assembly, and manufacturing implementation plan. National Science & Technology Council Washington, DC (2022)
2. Zhu, X., Zhang, C., Sun, R., Chen, J., Wan, X.: Orbit determination for fuel station in multiple SSO spacecraft refueling considering the J2 perturbation. Aerosp. Sci. Technol. **105**, 105994 (2020). https://doi.org/10.1016/j.ast.2020.105994
3. Schneider, J.: The time-dependent traveling salesman problem. Phys. A Stat. Mech. Appl. **314**(1–4), 151–155 (2002). https://doi.org/10.1016/S0378-4371(02)01078-6
4. Madakat, D., Morio, J., Vanderpooten, D.: Biobjective planning of an active debris removal mission. Acta Astronaut. **84**, 182–188 (2013). https://doi.org/10.1016/j.actaastro.2012.10.038
5. Apa, R., Hudson, J., Romano, M.: Request-centric modeling and architecture optimization for earth-moon space logistics. J. Spacecr. Rocket. (2025). https://doi.org/10.2514/1.A36495
6. Cerf, M.: Multiple space debris collecting mission: optimal mission planning. J. Optim. Theory Appl. **167**(1), 195–218 (2015). https://doi.org/10.1007/s10957-015-0705-0
7. Conway, B.A. (ed.): Spacecraft Trajectory Optimization. Cambridge University Press, Cambridge (2010)
8. Di Carlo, M., Vasile, M.: Analytical solutions for low-thrust orbit transfers. Celest. Mech. Dyn. Astron. **133**(7), 33 (2021). https://doi.org/10.1007/s10569-021-10033-9
9. Bourjolly, J., Gurtuna, O., Lyngvi, A.: On-orbit servicing: a time-dependent, moving-target traveling salesman problem. Int. Trans. Oper. Res. **13**(5), 461–481 (2006). https://doi.org/10.1111/j.1475-3995.2006.00558.x
10. Kanazaki, M., Yamada, Y., Nakamiya, M.: Trajectory optimization of a satellite for multiple active space debris removal based on a method for the traveling serviceman problem, pp. 61–66 (2017). https://doi.org/10.1109/IESYS.2017.8233562
11. Cerf, M.: Multiple space debris collecting mission—debris selection and trajectory optimization. J. Optim. Theory Appl. **156**(3), 761–796 (2013). https://doi.org/10.1007/s10957-012-0130-6
12. Gatto, G., Casalino, L.: Fast evaluation and optimization of low-thrust transfers to multiple targets. J. Guid. Control. Dyn. **38**(8), 1525–1530 (2015). https://doi.org/10.2514/1.G001116
13. Li, H., Chen, S., Baoyin, H.: J2-perturbed multitarget rendezvous optimization with low thrust. J. Guid. Control. Dyn. **41**(3), 802–808 (2018). https://doi.org/10.2514/1.G002889
14. Narayanaswamy, S., Wu, B., Ludivig, P., Soboczenski, F., Venkataramani, K., Damaren, C.J.: Low-thrust rendezvous trajectory generation for multi-target active space debris removal using the RQ-Law. Adv. Space Res. **71**(10), 4276–4287 (2023). https://doi.org/10.1016/j.asr.2022.12.049
15. Wijayatunga, M.C., Armellin, R., Holt, H., Pirovano, L., Lidtke, A.A.: Design and guidance of a multi-active debris removal mission. Astrodynamics **7**(4), 383–399 (2023). https://doi.org/10.1007/s42064-023-0159-3
16. Jorgensen, M.K., Sharf, I.: Optimal planning for a multiple space debris removal mission using high-accuracy low-thrust transfers. Acta Astronaut. **172**, 56–69 (2020). https://doi.org/10.1016/j.actaastro.2020.03.031
17. Di Carlo, M., Romero Martin, J.M., Vasile, M.: Automatic trajectory planning for low-thrust active removal mission in low-earth orbit. Adv. Space Res. **59**(5), 1234–1258 (2017). https://doi.org/10.1016/j.asr.2016.11.033
18. Zuiani, F., Vasile, M.: Preliminary design of debris removal missions by means of simplified models for low-thrust, many-revolution transfers. Int. J. Aerosp. Eng. **2012**, 1–22 (2012). https://doi.org/10.1155/2012/836250
19. Lee, D., Ahn, J.: Optimal multitarget rendezvous using hybrid propulsion system. J. Spacecr. Rocket. **60**(2), 689–698 (2023). https://doi.org/10.2514/1.A35540
20. Apa, R., Kaminer, I., Hudson, J., Romano, M.: Optimal low-thrust orbital transfer for servicing multiple satellites in elliptical orbits. Acta Astronaut. (2024). https://doi.org/10.1016/j.actaastro.2024.12.030
21. Cerf, M.: Optimal plan for multiple debris removal missions. RAIRO - Op. Res. **51**(4), 1005–1032 (2017). https://doi.org/10.1051/ro/2017009

22. Varga, G.I., Pérez, J.S.: Many-revolution low-thrust orbit transfer computation using equinoctial Q-law including J2 and eclipse effects. In: 6th International Conference on Astrodynamics Tools and Techniques, vol. 1, pp. 29–42. Darmstatd (2016)
23. Apa, R., Bhattacharjee, S., Hudson, J., Romano, M.: Optimal multi-client trajectory planning for a low-thrust servicing satellite in the presence of perturbations. J. Astronaut. Sci. **72**(2), 7 (2025). https://doi.org/10.1007/s40295-025-00487-6
24. Athans, M., Falb, P.L.: Optimal Control: An Introduction to the Theory and its Applications. Dover Books on Engineering, Dover Publications, New York (2007)
25. Edelbaum, T.N.: Optimum low-thrust rendezvous and station keeping. AIAA J. **2**(7), 1196–1201 (1964). https://doi.org/10.2514/3.2521
26. Li, H., Chen, S., Baoyin, H.: J2-perturbed multitarget rendezvous optimization with low thrust. J. Guid. Control. Dyn. **41**(3), 802–808 (2018). https://doi.org/10.2514/1.G002889
27. Zuiani, F., Vasile, M.: Preliminary design of debris removal missions by means of simplified models for low-thrust, many-revolution transfers. Int. J. Aerosp. Eng. **2012**, 1–22 (2012). https://doi.org/10.1155/2012/836250
28. Edelbaum, T.N.: Propulsion requirements for controllable satellites. ARS J. **31**(8), 1079–1089 (1961). https://doi.org/10.2514/8.5723
29. Kechichian, J.A.: Reformulation of Edelbaum's low-thrust transfer problem using optimal control theory. J. Guid. Control. Dyn. **20**(5), 988–994 (1997). https://doi.org/10.2514/2.4145
30. Kluever, C.A.: Using Edelbaum's method to compute low-thrust transfers with Earth-shadow eclipses. J. Guid. Control. Dyn. **34**(1), 300–303 (2011). https://doi.org/10.2514/1.51024
31. Chobotov, V.A., American Institute of Aeronautics and Astronautics (eds.): Orbital Mechanics, 3 edn. AIAA Education Series. American Institute of Aeronautics and Astronautics, Reston (2002)
32. Montenbruck, O., Gill, E.: Satellite orbits. Chap. 3. Springer, Berlin (2000). https://doi.org/10.1007/978-3-642-58351-3
33. Sumath R. M.: Computation of eclipse time for low-earth orbiting small satellites. Int. J. Aviat. Aeronaut. Aerosp. **6**(5) (2019). https://doi.org/10.15394/ijaaa.2019.1412
34. Press, W.H., Teukolsky, S.A., Vetterling, W.T., Flannery, B.P.: Numerical Recipes in C: the Art of Scientific Computing, Chap. 3, 2nd edn., pp. 91–139. Cambridge University Press, Cambridge (1995)
35. Salkin, H.M., De Kluyver, C.A.: The knapsack problem: a survey. Nav. Res. Logist. Q. **22**(1), 127–144 (1975)
36. Winter Althaus, G. (ed.): Genetic Algorithms in Engineering and Computer Science. Wiley, Chichester (1995)
37. Patterson, M., Benson, S.: Next ion propulsion system development status and performance. In: 43rd AIAA/ASME/SAE/ASEE Joint Propulsion Conference & Exhibit, p. 5199 (2007)
38. Izzo, D., Getzner, I., Hennes, D., Simões, L.F.: Evolving solutions to TSP variants for active space debris removal. In: Proceedings of the 2015 Annual Conference on Genetic and Evolutionary Computation, pp. 1207–1214. ACM, Madrid (2015). https://doi.org/10.1145/2739480.2754727

Authors and Affiliations

Riccardo Apa[1] · Jennifer Hudson[2] · Marcello Romano[3]

✉ Riccardo Apa
riccardo.apa@polito.it

[1] Mechanical and Aerospace Engineering Department, Politecnico di Torino, Corso Duca degli Abruzzi 24, 10129 Torino, Italy

[2] Mechanical and Aerospace Engineering Department, Western Michigan University, 1903 West Michigan Avenue, Kalamazoo, MI 49008, USA

[3] Chair of Astrodynamics, Technical University of Munich (TUM), Willy-Messerschmitt-Str. 11, 85521 Taufkirchen, Germany